Journal of Materials Science Research and Reviews

9(1): 44-54, 2022; Article no.JMSRR.85311

Structural, Morphological and Optical Characterization of Copper Antimony Sulphide $CuSbS_2$ Thin Film Deposited by Spin Coating for Photovoltaic Applications

Clement Sichangi [a*], Henry Barasa Wafula [a], Victor Odari [a] and Albert Owino Juma [b]

[a] Masinde Muliro University of Science and Technology, Kenya.
[b] Department of Education and Training Victoria, Melbourne, Australia.

Authors' contributions

This work was carried out in collaboration among all authors. All authors read and approved the final manuscript.

Article Information

Open Peer Review History:
This journal follows the Advanced Open Peer Review policy. Identity of the Reviewers, Editor(s) and additional Reviewers, peer review comments, different versions of the manuscript, comments of the editors, etc are available here: https://www.sdiarticle5.com/review-history/85311

Original Research Article

Received 20 January 2022
Accepted 29 March 2022
Published 31 March 2022

ABSTRACT

Solar energy is the most abundant renewable energy source on the earth surface. For many years, research has been done on making use of this source of energy. The current CdTe solar cell technology has good efficiency. However, large scale manufacture of CdTe PV modules are constrained due to the limited Te elemenet and the water soluble Cd element poses hazardous effects. The thickness of Cd has been reduced in the recent production from 3-8 nm to 0.5-1.28 nm but it remains poisonous and expensive. As an alternative, CIGS has been used but it is equally expensive. $CuSbS_2$ is a very potential none poisonous and more abundant absorber materials for thin film solar cells yet its potential has not been fully reached. In this research, a homogenous solutions of $CuSbS_2$ stochiometric ratio of 2.5:1 was deposited on a glass substrate by spin coating and then samples annealed at various temperatures ranging from 100 ^{0}C to 400 ^{0}C. X-ray diffraction showed that the control sample had amorphous structure as the crystallinity of annealed samples increased with increase in annealing temperatures. The d-spacing decreased with an increase in annealing temperature. Similarly, band gap energy decreased from 2.35 eV- 1.85 eV with an increase in annealing temperature. These results are in agreement with the earlier reports in literature.

**Corresponding author: Email: sichangiclement@gmail.com;*

Keywords: *Solar energy; renewable energy source; solar cell technology; thin film photovoltaic (TFPV); spin coating technique.*

1. INTRODUCTION

Energy crisis has been a great challenge in the present world scenario. Solar energy being renewable energy source and free can be used to meet the energy demand into the future. Photovoltaic cells are the technology used to convert solar energy into electrical energy. Among the various types of solar cells developed so far, thin film photovoltaic (TFPV) is the most viable technology to revolutionize the present cost of Si-based solar cells. Solar energy technology is therefore, growing rapidly owing to the fact that it is a clean, cheap and sustainable source.

Various materials have been fabricated in order to obtain more efficient solar cells. The major aim in the solar cells field is to obtain a device with low cost, low payback time and high efficiency and easy to process. The current thin film solar cell technologies based on CdTe and CIGS have issues which limited their application i.e are costly and some poisonous [1]. The increasing energy demand and the limitations of the existing technologies due to the scarcity, cost and toxicity of the materials urge the researchers to hunt for efficient thin film solar cells based on earth-abundant, inexpensive and less toxic materials.

For a decade, binary and ternary antimony based sulfides have gained attention due to their possible applications in solar cells. Due to the availability and low cost of the elements, the ternary Cu–Sb–S and Cu–Sb–Se semiconductor systems are being studied as sustainable alternative absorber materials to replace $CuIn(Ga)(S,Se)_2$ in thin film photovoltaic applications. $CuSbS_2$ is a very potential non-toxic, earth-abundant absorber material for thin film solar cells yet its photovoltaic related properties are yet to be exploited [2,3].

$CuSbS_2$ thin films through a solid state reaction process at 400^0C involving thin films of Sb_2S_3 (0.5 mm) and CuS obtained a direct optical band gap of 1.52 eV [4]. The characteristics reported here also offer perspective for $CuSbS_2$ as a potential absorber material in solar cell application. Limitations being the low minority carrier mobility arising from intrinsic behaviour of the material and due to the small crystalline grain size (20 nm) of the material produced. They then proposed consideration of a material of the type $Cu(Sb/Bi)(S/Se)_2$, prepared by annealing chemically deposited multi-layer semiconductor thin films, to overcome many of the limitations [5,6].

$CuSbS_2$ is a promising nontoxic and earth-abundant photovoltaic absorber that is chemically simpler than the widely studied Cu_2ZnSnS_4. However, it has relatively low efficiency and poor reproducibility, often due to suboptimal material quality and insufficient optoelectronic properties. To address these issues, thermochemical treatment (TT) for $CuSbS_2$ thin films was developed, which consists of annealing in Sb_2S_3 vapour followed by a selective KOH surface chemical etch. The annealed $CuSbS_2$ films show improved structural quality and optoelectronic properties, such as stronger band-edge photoluminescence and longer photo excited carrier lifetime. These improvements also lead to more reproducible $CuSbS_2$ PV devices, with performance currently limited by a large cliff-type interface band offset with CdS contact. Overall, these results point to the potential avenues to further increase the performance of $CuSbS_2$ thin film solar cell, and the findings can be transferred to other thin film photovoltaic technologies [7-9].

Optical studies revealed that $CuSbS_2$ material could be exploited for various purposes which include being used as an absorber material for the construction of solar cells, for the fabrication of optical devices and for the manufacture of highly reflective mirrors commonly found in desktop scanners, photocopy machines, halogen lamps, astronomical telescope and car head lamps [10]. The material was observed to have a direct band gap between 2.05 eV and 2.85 eV depending on the dip time. However, he did not touch on the effect of annealing on the structural properties of the material.

This paper reports on structural and morphological properties of $CuSbS_2$ thin films prepared by spin coating method. Spin coating is a cost effective wet chemical method that is fast, easy to manipulate and can be used for a wide range of materials.

2. EXPERIMENTAL TECHNIQUES

A 2M solution of $SbCl_3$ was prepared by dissolving 4.5626 grams of $SbCl_3$ in 20 ml of methanol at a temperature of 40 ^{0}C and stirred

continuously using a magnetic stirrer. This formed a brown solution. Similarly, a 2M $CuCl_2$ solution was prepared by dissolving 2.689 grams of $CuCl_2$ in 20 ml of ethanol at 60^0C while stirring continuously. This formed a green- yellow solution. Thiourea (2.69 grams) was dissolved in 100 ml of ethanol at 60^0C resulting a clear solution. To obtain SbS_2, 10 ml of $SbCl_3$ solution was mixed with 90 ml of thiourea solution. This formed a yellow solution. The SbS_2 solution was then mixed with the earlier prepared $CuCl_2$ solution in the ratio of $CuCl_2$:SbS_2, 2:1 forming a blue solution of $CuSbS_2$. The ratio was then adjusted to 2.5:1 and used for deposition

2.1 Deposition

The spin coating technique was used. The model of the spin coater was P6700. The spin coater was set to 1000 rpm to allow for spreading without splashing, then increased to 4000 rpm where it was maintained for 2 minutes to allow for even spreading before increasing to 8000 rpm and maintained for 2minutes for further spreading. The spinning then slowed down steadily up to zero in 4 minutes to allow for drying. This procedure was maintained for all samples.

2.2 Annealing

The thin film samples obtained above, were heat treated in a programmable oven model at different temperatures ranging from 100^0C, 200^0C, 300^0C and 400^0C for a period of 1 hour for each temperature. The annealed samples were then allowed to cool within the oven to room temperature before they were subjected to analysis. One sample was not annealed in order to be used as a control sample.

X- ray diffraction technique was employed in determination of the structure of the film. Bruker D2 Phaser X-ray diffractometer (XRD), with a 0.51418 nm source and Cukα radiation for the 2Θ range of 20^0 to 80^0 was used. The average grain size was estimated by Scherer's formula [11].

$$D = \frac{k\lambda}{\beta \cos\theta} \quad (1)$$

Where,

D- Crystallite size (nm)
k- 0.9 (Scherer constant)
λ- 1.5409nm (wavelength of the X-rays source)
β- Full Width at Half Maximum diffraction peak (radians)
ɵ- Peak position (radians).

Scanning Electron Microscopy (Zeiss Crossbeam 540FESEM- Microscope) operating at 2 kV was used to investigate the morphology of copper antimony sulfide ($CuSbS_2$) film.

Optical measurements were done using ultra violet- visible infra-red spectrophotometer, model UV-1800 (UV-VIS). The spectrophotometer was set at 380 nm to 1100 nm for both absorption and transmittance. The samples comprised of annealed and not annealed. Determination of band gap energy was done by Tauc plot.

$$ahv = k(hv - Eg) \quad (2)$$

Where $a\ is\ absorbance\ coefficient$
h- Planks constant
v- Frequency of incident uv radiation
k- Constant
E_g- Band gap energy

$$E_g = 1240/\lambda \quad (3)$$

3. RESULTS AND DISCUSSION

3.1 Crystal Structure of $CuSbS_2$

The Fig. 1, shows the X- ray diffractograms of $CuSbS_2$ treated under different temperatures. There is a general increase in average grain size; 7.8 nm to 12.7 nm with increase in annealing temperature. However, there is a decrease in d-spacing from 6.4 nm to 2.0 nm as the annealing temperature increases from 25 ^{0}C to 400 ^{0}C. The decrease in d-spacing is attributed to the fact that the samples becomes more crystalline and the grains become more compact in the lattice. A sample at 25 ^{0}C has the largest d-spacing attributed to its amorphous nature. Other researchers obtained grain size of 13 nm for $CuSbS_2$ at 150^0C using combinatorial thermal evaporation technique [12]. The grain size in the range of 7 nm to 52 nm for samples treated between 100 ^{0}C and 220 ^{0}C was also found in a vacuum using Horizontal Bridgman method in preparation of $CuSbS_2$ [13]. This finding is therefore, consistent with the earlier researches.

Table 1. Shows how d-spacing, strain and crystallite size in nm vary with annealing temperature

Temperature in (^{0}C)	Average d-spacing (nm)	Crystallite size (nm)
25	6.4	7.8
100	6.1	7.9
200	6.0	10.7
300	5.5	12.1
400	2.0	12.7

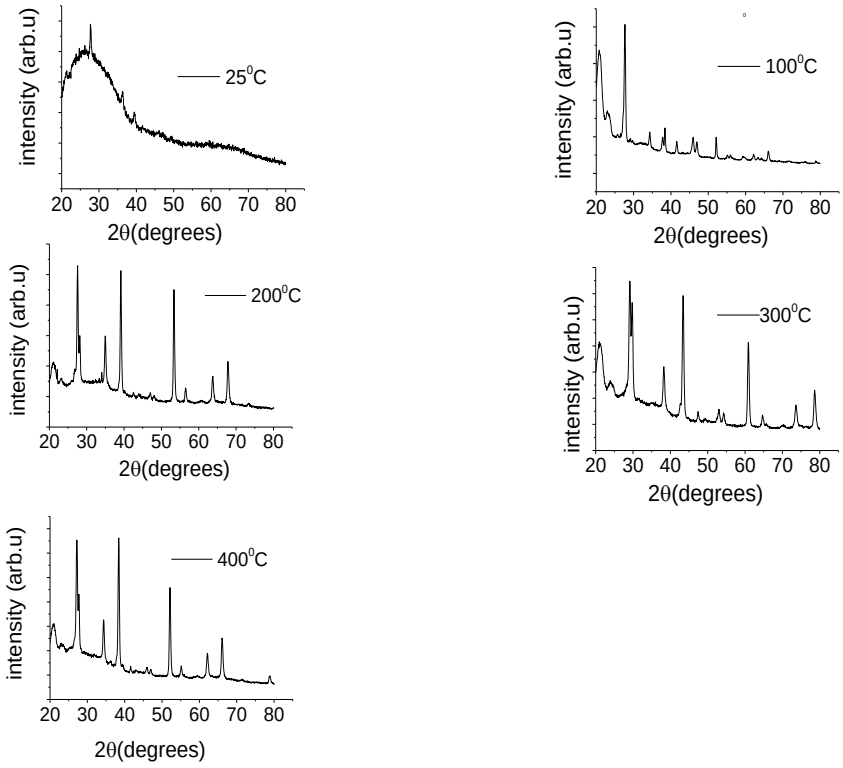

Fig. 1. The X- ray diffractograms of $CuSbS_2$ treated under different temperature

3.2 Morphology

The SEM pictures below, show cuboid shaped rods with an averaged dimension of 175 nm length and 53 nm width for a sample annealed at 100^{0}C. The rods are irregularly arranged. The irregular arrangement of these rods explains the large d-spacing in the sample at this temperature. However, the grains become more regular in the arrangement as the annealing temperature increases. This explains the decrease in d-spacing observed as the annealing temperature increases. A sample annealed at 200^{0}C, have grains that are cylindrical in shape with an average diameter of 22 nm. Other researchers reported nanorods of length 50 nm and diameter of 10 nm at annealing temperature of 200^{0}C [14], comparable to our finding here. At 300^{0}C, the sample is made up of cylindrical rods of an average length of 209 nm. At annealing temperature of 400^{0}C the crystals have an average dimensions of 107 nm. The measurements reported here are in agreement with earlier findings which reported lengths of 100-150 nm and d-spacing of 0.3 nm who prepared Cu_3SbS_3 nanorods by solvothermal approach and heat treated at 200^{0}C [15]. However, d-spacing of 0.3 nm is lower than what is reported in this findings of between 6.4 nm and 2.0nm due to the different stoichiometric ratio. The SEM images for $CuSbS_2$ annealed at different temperatures are shown below. The

samples treated at 200^{0}C. However, more are cylindrical as compared to those heat treated at 100^{0}C as shown in Figure (a) and Figure (b). The sample $CuSbS_2$ annealed at 300 ^{0}C has some voids in the structure likely attributed to uneven deposition. The areas highlighted in red shows neat compact structure that explains reduced d-spacing. While the areas highlighted in blue shows voids due to uneven deposition of the precursor. Figure (d) shows SEM image of $CuSbS_2$ annealed at 400^{0}C. The grains are more crystallined as compared to samples treated at lower temperatures.

3.3 Absorbance

The Fig. 3 show UV-VIS spectroscopy graph of absorbance against wavelenth of samples treated at different temperatures. The absorption of a sample heat treated at 100^{0}C was lower compared with samples heat treated at higher temperature. It exhibits sharp rise in absorption between the range of 800nm and 900nm wavelength of visible region. The sample treated at 200^{0}C show high absorption in this range. However, the absorption drops between the wavelength range of 400nm to 700nm before raising upto 900nm. Even with the drop, the values of absorbance remains high as compared to the samples treated at other temperatures. This raises the possibility of its application in solar cells. The samples treated at 300^{0}C and 400^{0}C equally show high absorbance in the visible region. K. Takei et. al (2014), reported decrease in absorption for wavelengths below 700nm. Similarly, R. Suriakarthic et. al (2015), reported decreasing absorption for the wavelengths below 800nm that is in agreement with the trend reported here. Therefore, the absorption reported here is in agreement with earlier report work.

Figure a) temp =100^{0}C

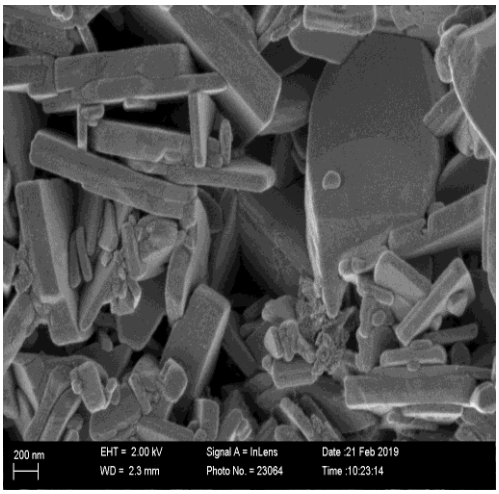

Figure b) temp = 200^{0}C

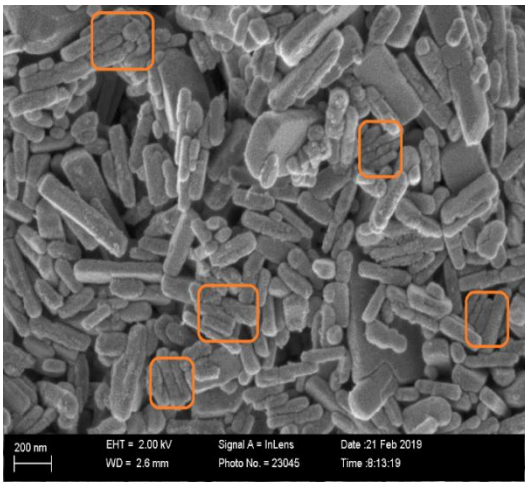

Figure c) temp =300^{0}C

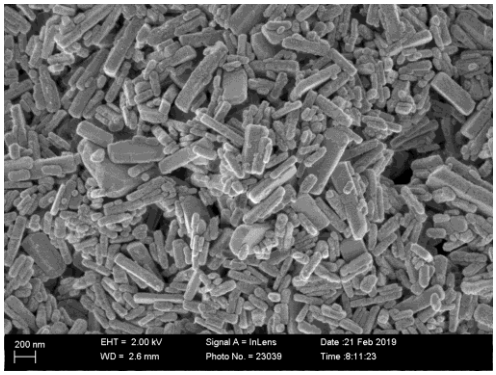

Figure d) temp =400^{0}C

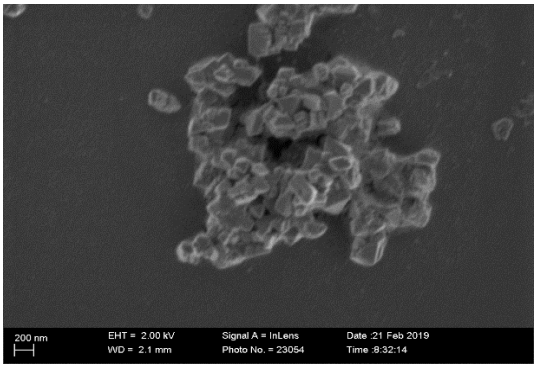

Fig. 2. SEM images

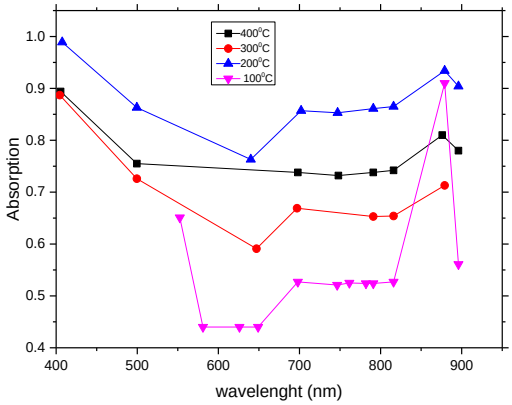

Fig. 3. Show absorbance of sample treated at various temperature for 1hr

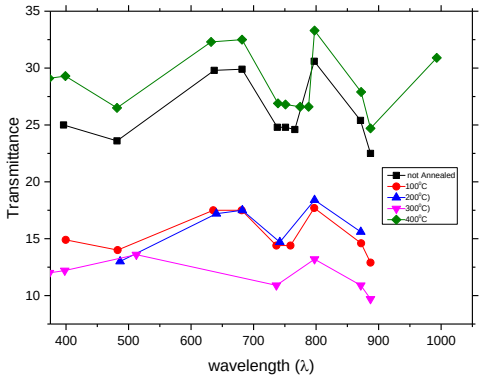

Fig. 4. Show transmittance of sample treated at various temperature for 1hr

3.4 Transmittance

The Fig. 4 show UV-VIS spectroscopy graph of transmittance against wavelenth of samples treated at different temperetures. The sample treated at 400^{0}C show highest transmittance of 27% with slight drop at 700nm wavelength region. A sample treated at 300^{0}C shows the lowest transmittance of 14% with a small peak at 800nm wavelength then a sharp drop to 9% at 900nm of wavelength. A sample treated at 200^{0}C shows an increasing transmittance from 12% - 18% in the region 500nm of wavelength with the highest transmittance at 800^{0}C. However, this transmittance is lower than one exhibited by samples at 400^{0}C that show 28% and not annealed sampled at 25%. A. Rabhi et. al (2014), reported transmittance of zero in wavelengths below 600nm that rises to 40% at 1800nm for samples treated up to 200^{0}C for 2hrs. Unlike this reported, we report transmittance above zero for samples at 25^{0}C 100^{0}C and 200^{0}C treated for 1hr. The difference can be attributed to the length of annealing time.

3.5 Reflectance

The Fig. 5 show UV-VIS spectroscopy graph of trreflectance against wavelenth of samples treated at different temperetures. The sample treated at 400^{0}C show highest reflectance of 53% with slight drop at wavelengths between 700nm-800nm and after 900nm. Similarly, not annealed sample show high reflectance of 49% with an increase to 52 % at 600nm. Samples annealed at 100^{0}C, 200^{0}C and 300^{0}C shows lower reflectance of 37%, 34% and 32% respectively, thus making them suitable for applications in solar cells. A. Rabhi et. al (2014), reported reflectance of 35% for sample treated at 200^{0}C that decreases with an increase in annealing temperature. The reflectance reported

here is in agreement with this report for temperatures above 100^{0}C but not for a sample at 25^{0}C which shows high reflectance. Similar report was given by K. Takei et. al (2014), however, with reflectance increasing with inncrease in the wavelength upto 60% at the wavelength of 1400nm.

3.6 Band Gap Analysis of CuSbS2 Annealed at Different Temperatures.S

Band gap energies were determined by TAUC plot, ahv against hv. Where the linear part of the plot was extrapolated to meet the energy axis at ahv =0. It was found that, the band gap energy generally reduces with annealing temperature. The sample treated at 25^{0}C, 100^{0}C and 400^{0}C show highest band gap energies of 2.35eV, 2.05eV and 2.05eV respectively. Samples treated at 200^{0}C and 300^{0}C exhibited same band gap energy of 1.95eV. Jeroh, D. M. (2012) previously reported that the band gap energies for CuSbS2 lies in the range of 1.30eV – 2.30eV. Similarly, N. Ali et. Al (2014), reported a band gap of 1.38-2.8eV for the samples treated between 100^{0}C and 400^{0}C. These values therefore, are in the range of earlier reported work.

3.6.1 Annealed at 25^{0}C

The Fig. 6 shows band gap energy for a sample treared at 25^{0}C. It has a direct band gap of 2.35eV.

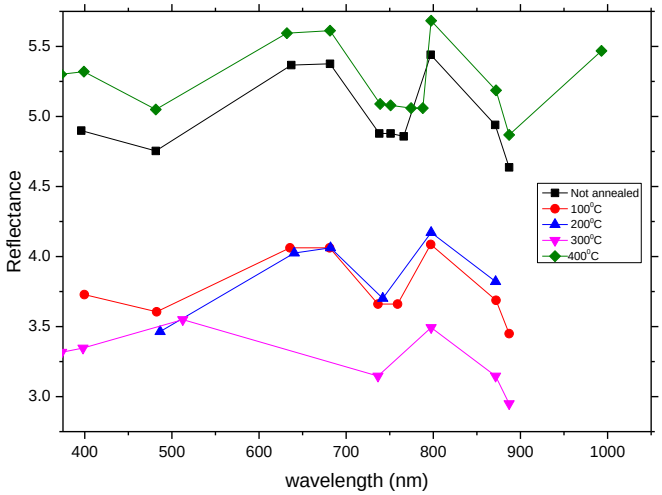

Fig. 5. Show transmittance of sample treated at various temperature for 1hr

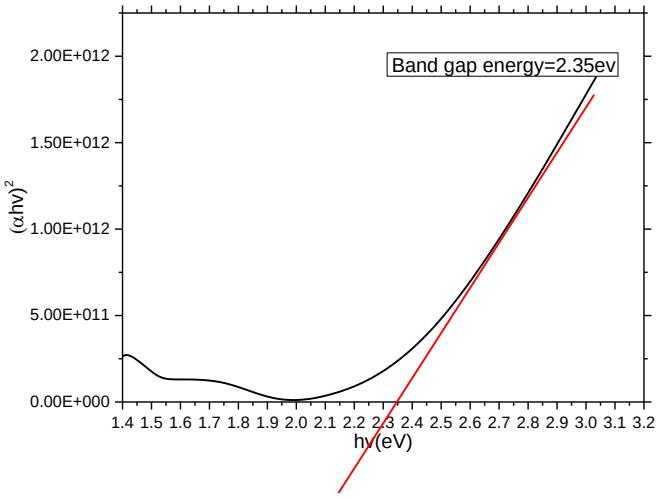

Fig. 6. Show band gap energy of a sample treated at 25^{0}C

3.6.2 Annealed at 100^{0}C

The Fig. 7 below shows band gap energy for a sample treared at 100^{0}C. It has a direct band gap of 1.9eV.

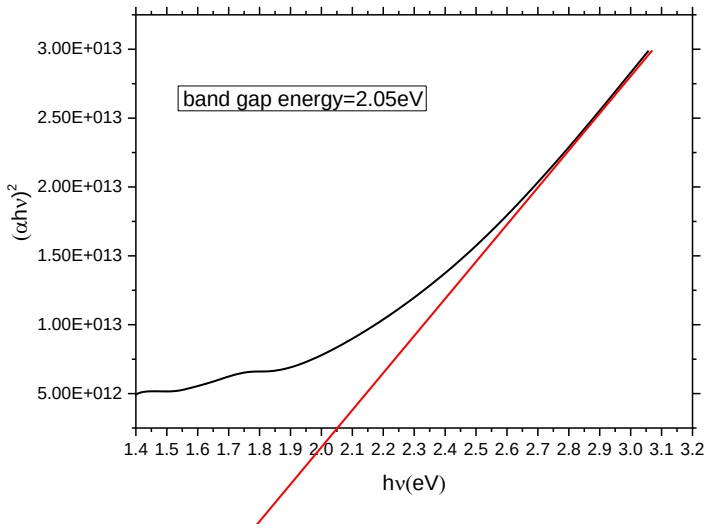

Fig. 7 Show band gap energy of a sample treated at 100^{0}C

3.6.3 Annealed at 200^{0}C

The Fig. 8 below shows band gap energy for a sample treared at 200^{0}C. It has a direct band gap of 1.85eV.

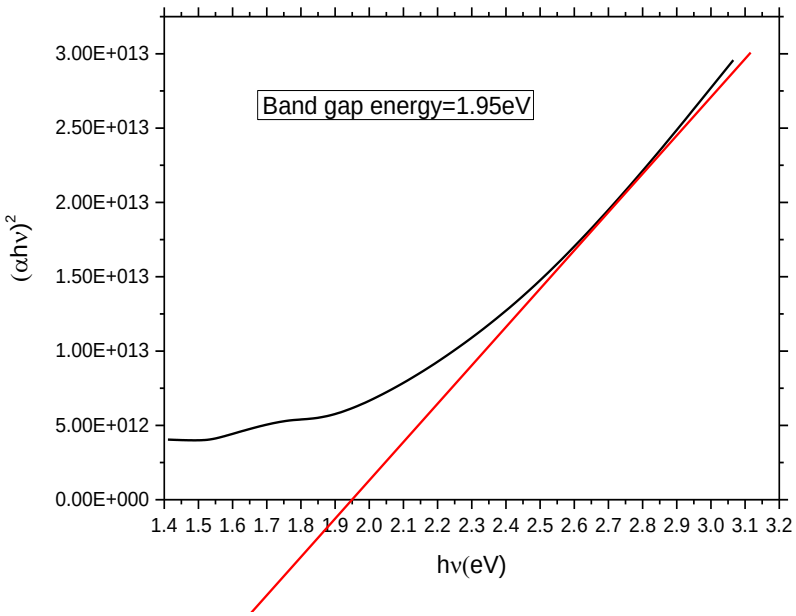

Fig. 8. Show band gap energy of a sample treated at 200^{0}C

3.6.4 Annealed at 300^{0}C

The Fig. 9 below shows band gap energy for a sample treared at 300^{0}C. It has a direct band gap of 1.85eV.

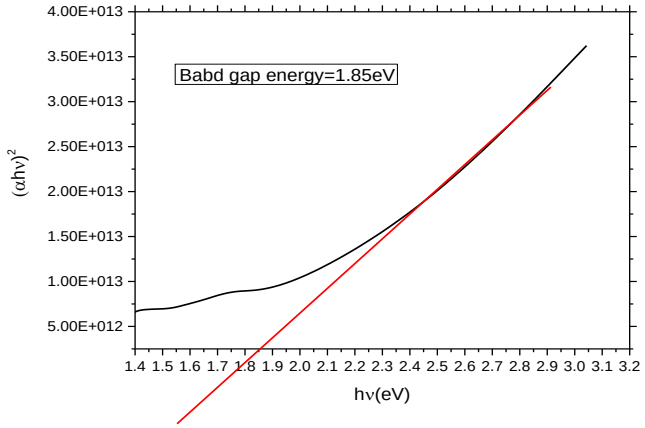

Fig. 9. Show band gap energy of a sample treated at 300^{0}C

3.6.5 Annealed at 400^{0}C

The Fig. 10 below shows band gap energy for a sample treared at 400^{0}C. It has a direct band gap of 2.05eV.

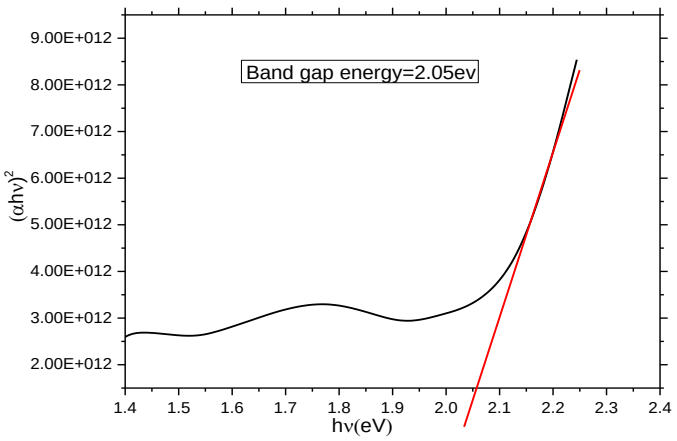

Fig. 10. Show band gap energy of a sample treated at 400^{0}C

Table 2. Variation of Band gap energy with annealing temperature

Annealing temperature (^{0}C)	Band Gap energy (eV)
25	2.35
100	2.05
200	1.95
300	1.95
400	2.05

4. CONCLUSIONS

In conclusion, $CuSbS_2$ was successfully prepared by spin coating technique. The samples were then subjected to post deposition heat treatment at different temperatures.

Structural and morphological analyses were done on the samples. XRD analysis shows that there is general increase in average grain size with increase in annealing temperature. The d-spacing decreased with an increase in annealing temperature. The sample not annealed was amorphous with very large d-spacing. As the crystallinity increases, the sample structure becomes more regular in the arrangement resulting to decrease in d-spacing as the annealing temperature increases. The SEM results shows a gradual change in the shape of the particles in the sample as the annealing temperature increases. Annealed samples were more regular in arrangement as compared to not annealed sample.

The samples treated at 25^0C and 400^0C had higher reflectance that can be applied in reflectors. While the sample treated at 300^0C had the lowest reflectance and therefore, can be used in solar cells. The band gap energy study showed that, the band gap energy generally reduces with annealing temperature between 2.35 eV and 1.85 eV. $CuSbS_2$ material is therefore a suitable absorber material and can be as well used as a suitable substitute to the conventional poisonous and rare earth compounds currently in use.

COMPETING INTERESTS

Authors have declared that no competing interests exist.

REFERENCES

1. Bo Y, Liang W, Jun H, Ying Z, Huaibing S, Shiyou C, Jiang T. CuSbS2 as promsing earth-abundant photovoltaic absorber material: A combined theoritical and experimental study. Chemistry of Materials. 2014;3135-3143.
2. Wafula HB. Characterization of cobalt doped titanium dioxide and Cu: In_2S_3 nanocomposite thin films deposited by ILGAR technique for photovoltaic application, PhD Thesis, Masinde Muliro University of Science and Technology; 2015.
3. Jeroh Diemiruaye M. An analytical study of the optical properties of copper antimony sulphide thin films and possible applications of the thin film; 2012.
4. Colombara D, Peter L, Rodgers K, Painter J, Roncallo S. Formation of CuSbS2 and CuSbSe2 thin films via chalcogenisation of Sb–Cu metal precursors. Thin Solid Films. 2011;7438–7443.
5. Rabhi, et al. Investigation on dispersive optical constant and microstructural parameters of the absorber $CuSbS_2$ thin films; 2015.
6. Arshad Hussain, et al. Post annealing effect on structural, optical and electrical properties of $CuSbS_2$ thin films fabricated by combinatorial thermal evaporation technique; 2015.
7. Rastogi A, Janardhana N. Properties of CuSbS2 thin films electrodeposited from ionic liquids as p-type absorber for photovoltaic solar cells. Thin Solid Films. 2014;0040-6090.
8. Rodriquiz-Lazcano Y, Nair K. CCuSbS2 thin films formed through annealing chemically deposited Sb2-S3Cus Thin Films. Crystal growth. 2011;399-406.
9. Satoshi S, Keisuke H, Masayoshi Y, Tooru T, Katsuhiko F, Yoichi I, Tetsuya K. Synthesis of cooer-antimon sulfide nanocrystals for solution processed solar cells. Inorganic Chemistry. 2015;7840-7845.
10. Diemiruaye J. Analytical study of optical properties of copper antimony sulfide thin films and possible applications of thin film. International Journal of Thin Films and Technology. 2012;0-66.
11. Francisco WD, Welch AW, Lauryn B, Patricia D, Hannes H, Thomas U, Andriy Z. Effect of thermochemical treatment on CuSbS2 photovoltaic absorber quality and solar cell reproducibility. Physical Chemistry. 2016;18377-18385.
12. Garzaa C, Shajib S, Aratob A, Perez T, Alan C, Das R, Krishnanb. p-Type CuSbS2 thin films by thermal diffusion of copper into Sb2S3. Solar Energy Materials and Solar Cells, 2001-2005; 2010.
13. Liang W, Bo Y, Zhe X, Meiying L, Ying Z, Ding-Jiang X, Jiang T. Synrthesis and characterization of hydrazine soultion processed by CU12Sb4S13. Solar Energy Materials and Solar cells. 2016;33-39.

14. Mukesh K, Clas P. Cu(Sb,Bi)(S,Se)2 as indium-free absorber material with high optical efficiency. Energy Procedia. 2013; 176-183.

15. Zhong, et al. A sample L-Crystal – assisted solvothermal approach to Cu_3SbS_3 nanorods; 2010.

Peer-review history:
The peer review history for this paper can be accessed here:
https://www.sdiarticle5.com/review-history/85311